Microchimica Acta (2019) 186: 17
https://doi.org/10.1007/s00604-018-3138-2

ORIGINAL PAPER

Gold nanorods decorated with graphene oxide and multi-walled carbon nanotubes for trace level voltammetric determination of ascorbic acid

Yiwei Zhao[1] · Jianhua Qin[1] · Hui Xu[1] · Shanmin Gao[1] · Tingting Jiang[2] · Shengxiao Zhang[1] · Juan Jin[1]

Received: 24 August 2018 / Accepted: 1 December 2018 / Published online: 12 December 2018

Abstract

An ultra-sensitive sensor is described for the voltammetric determination of ascorbic acid (AA). A glassy carbon electrode (GCE) was modified with graphene oxide (GO), multi-walled carbon nanotubes (MWCNTs) and gold nanorods (AuNRs). GO was used to prevent the aggregation of MWCNTs. The integration of positively charged AuNRs reduces the overpotential and increases the peak current of AA oxidation. Figures of merit of this sensor, typically operated at a low working potential of 0.036 V (vs. Ag/AgCl), include a low detection limit (0.85 nM), high sensitivity (7.61 $\mu A \cdot \mu M^{-1} \cdot cm^{-2}$) and two wide linear ranges (from 1 nM to 0.5 μM and from 1 μM to 8 mM). The use of GO simplifies the manufacture and results in a highly reproducible and stable sensor. It was applied to the quantification of AA in spiked serum.

Keywords Electrochemical sensor · Modified electrode · Hybrid material · Electrocatalysis · Differential pulse voltammetry

Introduction

Carbon based material [1–5] and noble metals [3, 6, 7] have sparked much interest owing to their excellent physical and chemical properties. However, improvement in sensitivity, linear ranges and selectivity are still the current analytical challenges. Carbon nanotubes (CNTs) are the ideal building blocks for molecular nanoelectronics due to its excellent in-plane conductivity, high surface-to-volume ratios and remarkable mechanical properties [8, 9]. However, the poor solubility of CNTs in solvent, especially in water hinders its further application. Therefore, considerable efforts have been focusing on increasing the solubility by functionalizing the surface of CNTs. However, it needed complex synthesis step and sometimes the functionalization may change the initial properties of CNTs [10]. Surprisingly, another carbon nanomaterial, the derivative of graphene, graphene oxide (GO), have been reported to be used as surfactant to disperse CNTs. [11–13] After addition of GO into CNT, reduction reaction was followed to restore the graphene structure to obtain reduced GO [14, 15]. Reduced GO is conductive while GO with many oxygen-containing functional groups [16] is nonconductive and can increase the resistance of charge transfer [17]. However, some groups found that GO showed high electrocatalytic oxidation of some molecules including AA [18], DA [19], dihydroxybenzene isomers and L-methionine [20]. Moreover, GO can improve the film-forming property of modified electrodes due to its own many hydrophilic groups. So, the incorporation of GO with CNT may not only increase the dispersibility of CNT but also render this hybrid material as a versatile platform for the electrocatalytic applications with improved efficiency. Moreover, the preparation process is simplified and eco-friendly because any toxic reductants did not be used. Last but not least, inactivation of catalysts (CNTs) caused by aggregation can be avoided.

On the other hand, gold nanorods (AuNRs) have exhibited high potential in electrocatalytic detection of small molecules [21]. The two-dimensional (2D) plane structure of GO can provide a vast platform for loading various nanoparticles to construct electrochemical sensors with improved performance [22, 23]. In this manuscript, instead of reduced GO, GO with combination of multi-walled carbon nanotubes

Yiwei Zhao and Jianhua Qin contributed equally to this work.

Electronic supplementary material The online version of this article (https://doi.org/10.1007/s00604-018-3138-2) contains supplementary material, which is available to authorized users.

✉ Hui Xu
xuhui235@163.com

[1] School of Chemistry and Materials Science, Ludong University, Yantai 264025, People's Republic of China

[2] College of Life Sciences, Ludong University, Yantai 264025, People's Republic of China

(MWCNTs) and AuNRs were used for the detection of ascorbic acid (AA). GO was added into MWCNTs aqueous solution to improve the dispersibility via non-covalent π-stacking interactions. After the glassy carbon electrode (GCE) was modified with GO and MWCNTs mixture, positively charged AuNRs was further modified. A synergistic effect on the electrocatalytic oxidation of AA with decreased overpotential and greatly increased sensitivity was successfully achieved.

Experimental

Chemicals

MWCNTs were purchased from Shenzhen Nanotech Port Ltd., China (purity >95%). Chloroauric acid hydrate ($HAuCl_4 \cdot 4H_2O$) and D-(+)-glucose (Glu) anhydrous were acquired from Sinopharm Chemical Reagent Co., Ltd. (http://en.reagent.com.cn/). L-AA (>99.7%) was purchased from Tianjin Ruijin Special Chemicals Reagent Co., Ltd. (http://www.cndss.net/company-tianjinshiruijintehuaxuepin656.html). Dopamine hydrochloride (DA·HCl), L-Glutatione reduced (L-GSH, >98.0%), hexadecyl trimethyl ammonium bromide (CTAB, >99.0%) were purchased from Sigma-Aldrich (www.sigmaaldrich.com) and uric acid (UA) from Alfa Aesar (https://www.alfa.com/zh-cn/). All other chemicals were analytical grade and used directly without further purification. All the solutions were prepared using ultrapure water (conductivity of 18.25 MΩ·cm).

Apparatus and instruments

Cyclic voltammetry (CV), differential pulse voltammetry (DPV) and electrochemical impedance spectroscopy (EIS) were recorded in a CHI-660C electrochemical workstation (CH Instrument, Shanghai, China, http://www.chinstr.com/). A conventional three-electrode system consists of an Ag/AgCl electrode as a reference, a Pt wire as auxiliary electrode and a modified GCE (3 mm in diameter) as working electrode. The surface morphologies of composites electrode were observed on a high resolution field emission scanning electron microscopy (FESEM, SU 8010, Hitachi, Japan, http://www.hitachi.com.cn/). The morphologies of MWCNTs, GO and AuNRs were conducted on the transmission electron microscopy (TEM, JEM-1230, JEOL, https://www.enfsolar.com/directory/equipment/21516/jeol) at an acceleration voltage of 100 kV. A UV2550 Spectrometer (Shimadzu, Japan, https://www.shimadzu.com.cn/) was used to obtain the absorption spectra of AuNRs. Raman spectra were performed using a Horiba spectrometer (LabRAM HR Evolution, Japan, http://www.horiba.com/cn/) set to an excitation wavelength of 532 nm.

Preparation of graphene oxide (GO) and gold nanorods (AuNRs)

Graphite oxide was prepared by the Hummers' method [24].

AuNRs were prepared by seeded growth method with moderate modification [25, 26] (detailed synthesis procedure was described in Electronic Supporting Material).

Construction of the sensors

Firstly, mixture of 1.0 $mg \cdot mL^{-1}$ MWCNTs and 1.0 $mg \cdot mL^{-1}$ GO aqueous solution was ultrasonically treated for several hours to obtain MWCNT/GO suspension. Prior to modification, GCE was sequentially polished with 1.0 μm, 0.3 μm and 0.05 μm Al_2O_3 powder to a mirror finish, followed by ultrasonication in ethanol and ultrapure water for 1.0 min, respectively. After the GCE was dried under a nitrogen stream, 5 μL of prepared MWCNT/GO suspension was directly dropped onto the GCE and then dried at 50 °C to assemble a MWCNT/GO layer on the GCE surface. Then 3 μL of AuNRs solution were directly added on the surface of MWCNT/GO and dried at 80 °C. The dropping of 3 μL AuNRs and drying were repeated it for 3 times to obtain homogeneous and adequate covering. The prepared modified GCE is named as MWCNT/GO/AuNR/GCE. CV (−0.2 ~ 0.6 V) and DPV (−0.3 ~ 0.4 V, amplitude of 50 mV, pulse period of 0.5 s, pulse width of 0.2 s) were performed in 0.1 M phosphate buffered saline (including 0.1 M NaCl, pH 7.4) containing different concentration of AA or other small molecules. Each CV or DPV experiment was repeated in triplicate, and the error bars indicated the calculated standard deviation. EIS was performed in an electrolyte solution of 5 mM $[Fe(CN)_6]^{4-/3-}$ containing 0.1 M KCl at the frequency range from 0.01 Hz to 100 kHz with amplitude of 5 mV. Init E was open circuit potential given by instrument. For real sample analysis, prior to the measurements, 1 mL of fresh human serum was mixed with 50 mL of phosphate buffered saline (pH 7.4) and used without any additional treatment. Then, known amount of standard AA (100 μM, 0.1 μM and 0.001 μM) was directly added into the above diluted real samples, respectively. DPV was performed at a working potential of 0.036 V (vs. Ag/AgCl). According to the current value, detected concentration can be found from the linear regression equations. From the detected concentration and the added standard concentration, recovery rate was calculated.

Results and discussion

Choice of materials

As demonstrated in the introduction, various kinds of nanomaterials have been applied to detect small molecules

by electrocatalysis [1–7, 14, 27–31]. CNTs were selected because it owns excellent conductivity, large specific surface area and electrocatalytic performance. The MWCNT/GO/AuNR nanocomposites modified GCE was prepared by a deposition process. GO, a unique two-dimensional (2D) hexagonal lattice structure, has many ionizable edge groups such as -OH, -COOH on its surface, having excellent water dispersity and chemical stability. Moreover, it has a lot of hydrophilic groups and the film-forming property of modified electrodes can be improved. Some literatures have reported the zeta potential value of GO, which was negative in the pH range 2–10 [32, 33]. It can be used as surfactant to disperse CNTs [11–13], which can prevent the aggregation of CNTs and improve the electrocatalytic performance of CNTs. Moreover, the 2D plane structure of GO can load various nanoparticles to construct electrochemical sensors with improved performance [22, 23]. After CNT/GO dispersion was dropped onto the surface of GCE, positively charged AuNRs with high conductivity and electrocatalytic performance were added on the surface of CNT/GO composites. CNT/GO/AuNR nanohybrid modified GCE was prepared due to the high affinity of negatively CNT/GO and AuNRs, leading to synergistically electrocatalytic response to AA oxidation. Although gold nanoparticles also own good electrocatalytic activity, AuNRs were selected here due to the electrostatic loading of it to the surface of CNT/GO composites with opposite charges. Moreover, AuNRs possess high surface area with efficient mass transport characteristics and favourable biocompatibility [21]. The sensitivity and selectivity of the electrochemical sensors thus can be further improved.

Characterization of prepared AuNRs

Since AuNRs can improve both of electrical conductivity and signal amplification for electrochemical detection of small molecules. The successful synthesis of AuNRs is a key factor for the prepared sensor. First, UV-visible spectra was used to confirm the formation of AuNRs. As shown in Fig. 1a, an absorption peak centered at 527.5 nm exhibited the formation of gold seed nanoparticles, which is the characteristic surface plasmon resonance absorption of seed nanoparticles. After $AgNO_3$ was introduced to the gold solution which is prepared via the reduction of $HAuCl_4$ with AA, the seed solution was added to the Au^+ stock solution in the presence of CTAB. A new plasmon band at 779 nm appeared (Fig. 1b), demonstrating the formation of AuNRs. From TEM images, the aspect ratio about 2.2 of AuNRs (calculated from 300 AuNRs) with a small fraction of the spherical nanoparticles was observed (Fig. 1c).

Characterization of prepared MWCNT/GO/AuNR nanohybrid

The morphologies of MWCNTs and MWCNT/GO dispersion were observed by TEM. As shown in Fig. 2a, b, intertangling MWCNTs with the average diameter of 10–20 nm (calculated from 150 MWCNTs) and well-dispersed MWCNTs between GO sheets for MWCNT/GO were observed. Moreover, the successful modification of the GCE was confirmed by FESEM studies (Fig. 2c, d, and e). Figure 2c represents the modified GCE by MWCNTs, and intertangling, inhomogeneous, and aggregated structure can be observed. For MWCNT/GO modified GCE, uniform modification can be found without obvious aggregation (Fig. 2d). For MWCNT/GO/AuNR modified GCE, an unclear interface can be observed due to a large amount of precipitated CTAB used in the preparation of AuNRs (Fig. 2e).

Raman spectra of MWCNTs (1), MWCNT/GO (2), MWCNT/GO with 5 μL AuNRs (3) and 10 μL AuNRs (4) are shown in Fig. 2f. Raman spectra of MWCNTs show two obvious bands at 1593 cm^{-1} and 1348 cm^{-1}, which are attributed to the *G* mode (a Raman-allowed phonon high-frequency mode) and *D* mode (a disordered-induced peak) [34]. The I_G/I_D ratios change for different samples, which are 0.94 for MWCNT, 0.89 for MWCNT/GO, 0.72 for MWCNT/GO/AuNR (5 μL), 0.69 for MWCNT/GO/AuNR (10 μL), demonstrating the increase of the denominator *D*-band. I_G/I_D ratio decreases due to addition of GO and attachment of AuNRs on

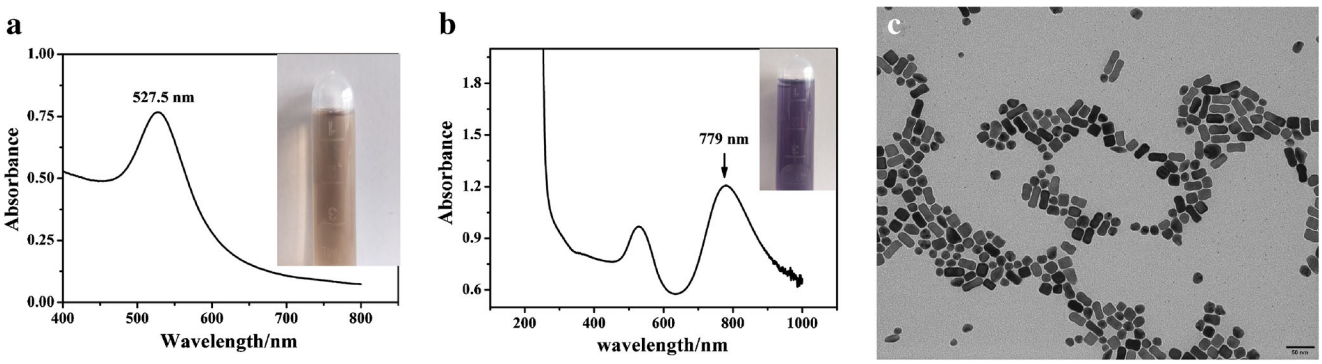

Fig. 1 The UV-Vis spectra of gold nanoparticles (**a**), AuNRs (**b**), and TEM images for prepared AuNRs (**c**). The inset of A is brown gold nanoparticles, and inset of B is blue-purple AuNRs

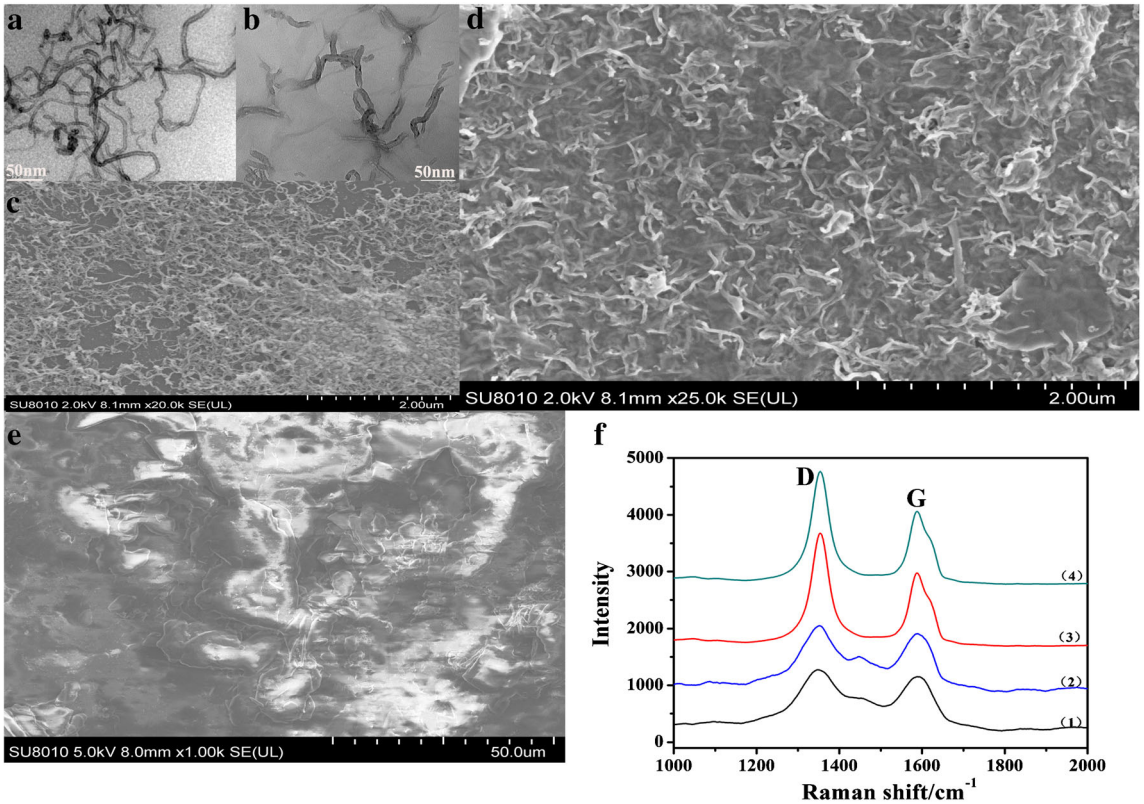

Fig. 2 TEM images for MWCNTs (**a**) and MWCNT/GO (**b**). FESEM images for MWCNTs modified GCE (**c**), MWCNT/GO modified GCE (**d**), and MWCNT/GO/AuNR modified GCE (**e**). Raman spectra (**f**) of MWCNTs (1), MWCNT/GO (2), MWCNT/GO with 5 μL AuNRs (3) and 10 μLAuNRs (4)

the surface of the MWCNT/GO, confirming the successful modification of the GCE by MWCNT/GO/AuNR composite.

Electrochemical properties of MWCNT/GO/AuNR/GCE

Interfacial properties of the surface-modified electrodes were studied by EIS. The charge-transfer resistance (Rct) at the electrode surface is equal to the diameter of semicircle. Figure 3a shows the impedance spectra of the bare GCE (a), MWCNT/GO /AuNR/GCE (b), MWCNT/GCE (c) and MWCNT/GO/GCE (d) in 5 mM $K_3Fe(CN)_6$ and $K_4Fe(CN)_6$ containing 0.1 M KCl. It can be seen that the semicircle of the bare GCE is larger, indicating a greater resistance between the electrolyte and electrode. MWCNTs modified GCE exhibits a small diameter, suggesting a faster electron-transfer rate and lower Rct due to the excellent conductivity of MWCNTs. By

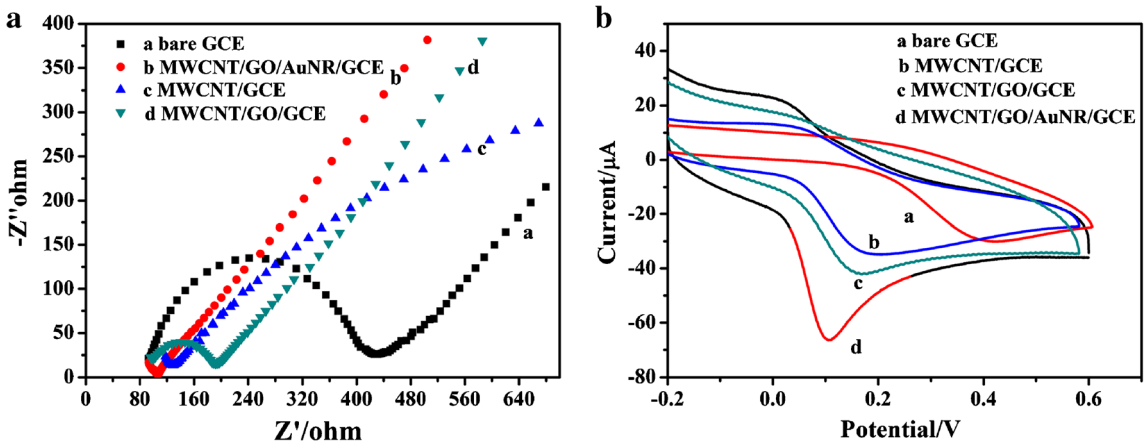

Fig. 3 **a** EIS curves of bare GCE (a), MWCNT/GO/AuNR/GCE (b), MWCNT/GCE (c), MWCNT/GO/GCE (d) in 5 mM $K_3Fe(CN)_6$ and $K_4Fe(CN)_6$ containing 0.1 M KCl. **b** CVs of (a) bare GCE, (b) MWCNT/GCE, (c) MWCNT/GO/GCE and (d) MWCNT/GO/AuNR/GCE containing 8 mM AA in phosphate buffer (including 0.1 M NaCl, pH 7.4) at temperature 55 °C (scan rate of 100 mV s^{-1})

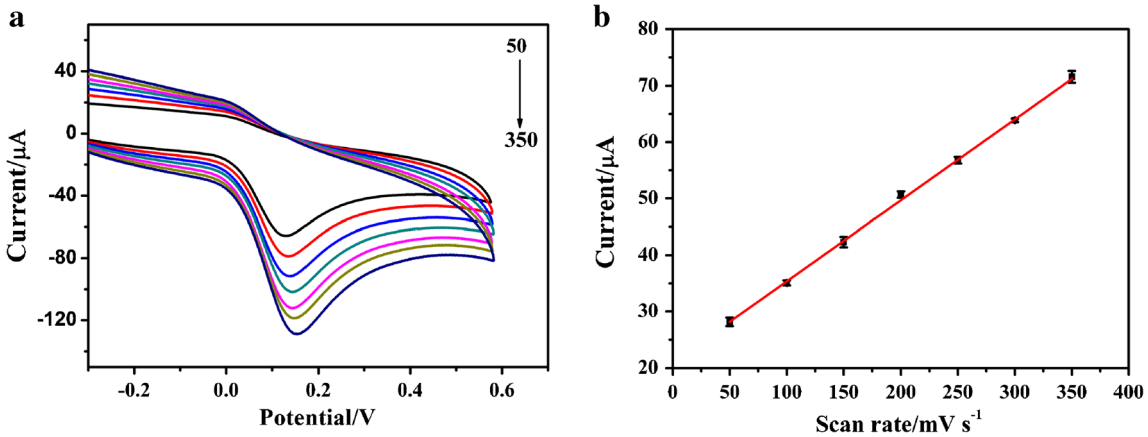

Fig. 4 **a** CVs of the MWCNT/GO/AuNR/GCE in phosphate buffered saline (pH 7.4) with 8 mM AA at different scan rates (50, 100, 150, 200, 250, 300 and 350 mV s^{-1}). **b** The variation of the oxidation peak currents vs. scan rate

contrast, MWCNT/GO modified GCE exhibits a little bigger semicircle than that of MWCNTs modified GCE due to the insulating property of GO and the electrostatic repulsion of negatively charged GO and $Fe(CN)_6^{3-}/Fe(CN)_6^{2-}$. Similar results have been reported previously [35]. At last, MWCNT/GO/AuNR modified electrode exhibits the minimum Rct due to the synergistic interaction of MWCNT/GO and conductive AuNRs. In addition, positively charged AuNRs decrease the electrostatic repulsion between the modified electrode and redox probe. Furthermore, the active surface area of all electrodes can be found by CV at different scan rates using 5.0 mM $K_3Fe(CN)_6$ as a probe (data not shown). According to the Randles-Sevcik equation, the average electroactive areas of GCE, MWCNT/GCE,

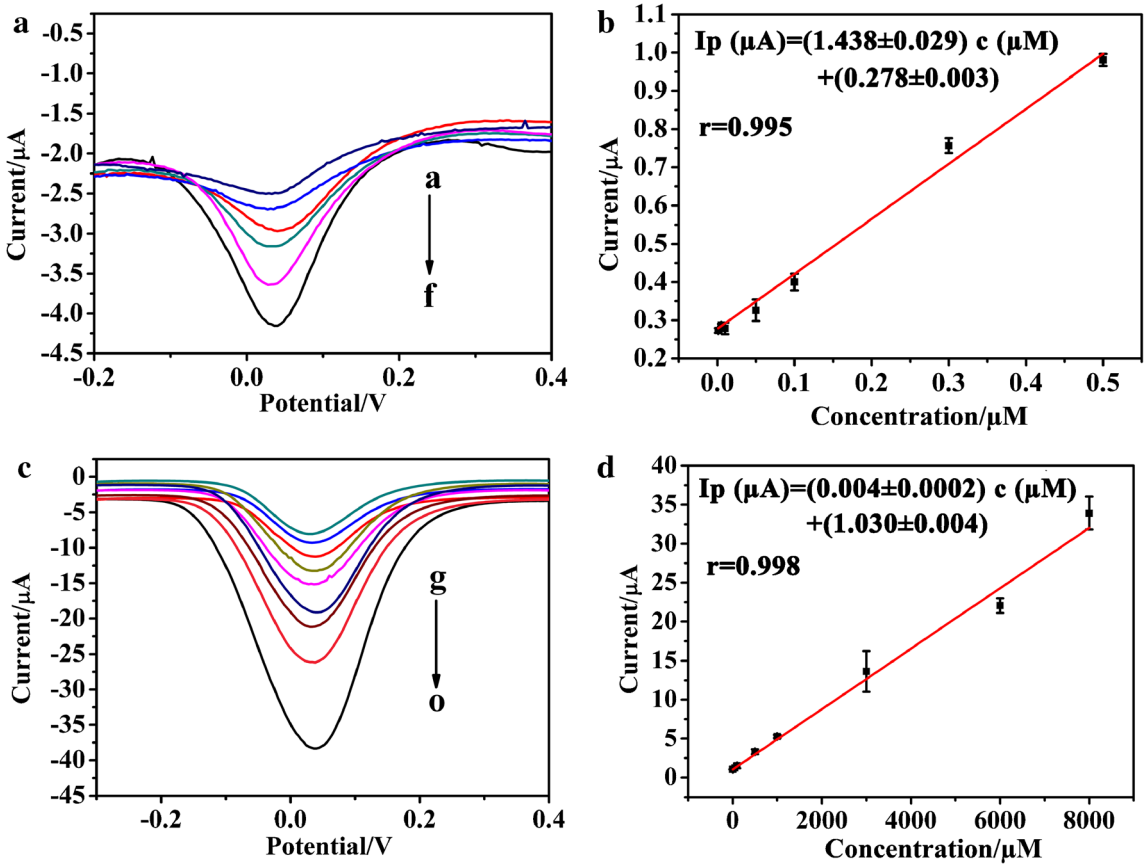

Fig. 5 DPV of MWCNT/GO/AuNR/GCE for different concentrations of AA from 1 nM to 0.5 μM (curve a to curve f) (**a**), and 1 μM to 8 mM (curve g to curve o) (**c**) in phosphate buffer (including 0.1 M NaCl, pH 7.4) at temperature 55 °C. Plot of peak current versus AA concentration from 1 nM to 0.5 μM (**b**), and 1 μM to 8 mM (**d**) at working potential of 0.036 V (vs. Ag/AgCl)

GO/GCE, MWCNT/GO/GCE, and MWCNT/GO/AuNR /GCE were calculated to be 0.0700, 0.123, 0.137, and 0.189 cm^2, respectively. The results above suggest that AuNRs integrated with MWCNT/GO hybrid yielded a higher electroactive area.

Moreover, the electrochemical properties of various electrodes were studied using CV from −0.20 to 0.60 V in the presence of 8 mM AA in 0.1 mol·L^{-1} phosphate buffered saline at pH 7.4. It can be found from Fig. 3b that bare GCE only had weak response signal with a big overpotential to AA. MWCNTs modified GCE showed an increased oxidation peak current and obviously decreased overpotential because MWCNTs exhibit excellent electrical conductivity and good electrocatalytic performance toward AA. Compared with MWCNTs modified GCE, MWCNT/GO modified GCE showed a little larger current response and negatively shifted oxidation potential. By contrast, when MWCNT/GO/AuNR/GCE was used to detect AA at the same concentration, the biggest oxidation peak current and the greatly decreased overpotertial was found (from 0.399 V for bare GCE to 0.11 V for MWCNT/GO/AuNR/GCE). It indicates that GO/MWCNT/AuNR possesses outstanding electrocatalytic activities to AA in phosphate buffer. The reason is that the synergistic action of well-dispersed MWCNT/GO with large specific surface area and AuNRs with outstanding electrical conductivity and electrocatalytic performance.

Optimization of method

The following parameters were optimized: (a) sample pH value; (b) temperature. Respective data and Figures are given in the Electronic Supporting Material. In short, the following experimental conditions were found to give best results: (a) Best sample pH value: 7.4; (b) Optimal temperature: 55 °C.

The effect of scan rate

Figure 4a shows the CVs of the GO/MWCNT/AuNR modified GCE in the presence of 8 mM AA at various scan rates at 55 °C in 0.1 M phosphate buffer (including 0.1 M NaCl, pH 7.4). The oxidation peaks current increased with increased scan rates from 50 mV s^{-1} to 350 mV s^{-1}. The anodic peak current is proportional to the scan rate and the linear equation is I_p (μA) = (0.1434 ± 0.0021) V (mV s^{-1}) + (20.9975 ±

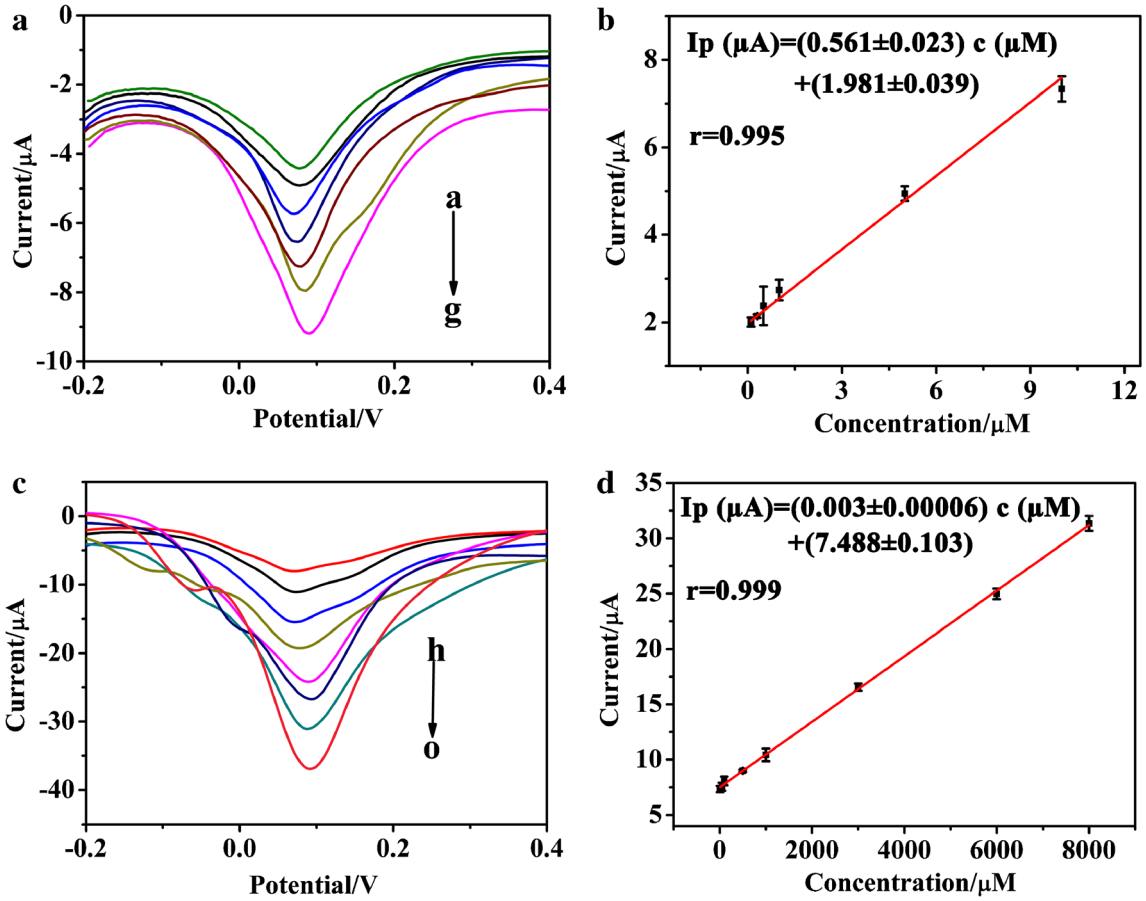

Fig. 6 DPV of MWCNT/GO/AuNR/GCE for different concentrations of AA from 0.1 μM to 10 μM (curve a to curve g) (**a**), and 10 μM to 8 mM (curve h to curve o) (**c**) in 0.1 M phosphate buffer (including 0.1 M NaCl, pH 7.4) at room temperature. Plot of peak current versus AA concentration from 0.1 μM to 10 μM (**b**), and 10 μM to 8 mM (**d**) at working potential of 0.086 V (vs. Ag/AgCl)

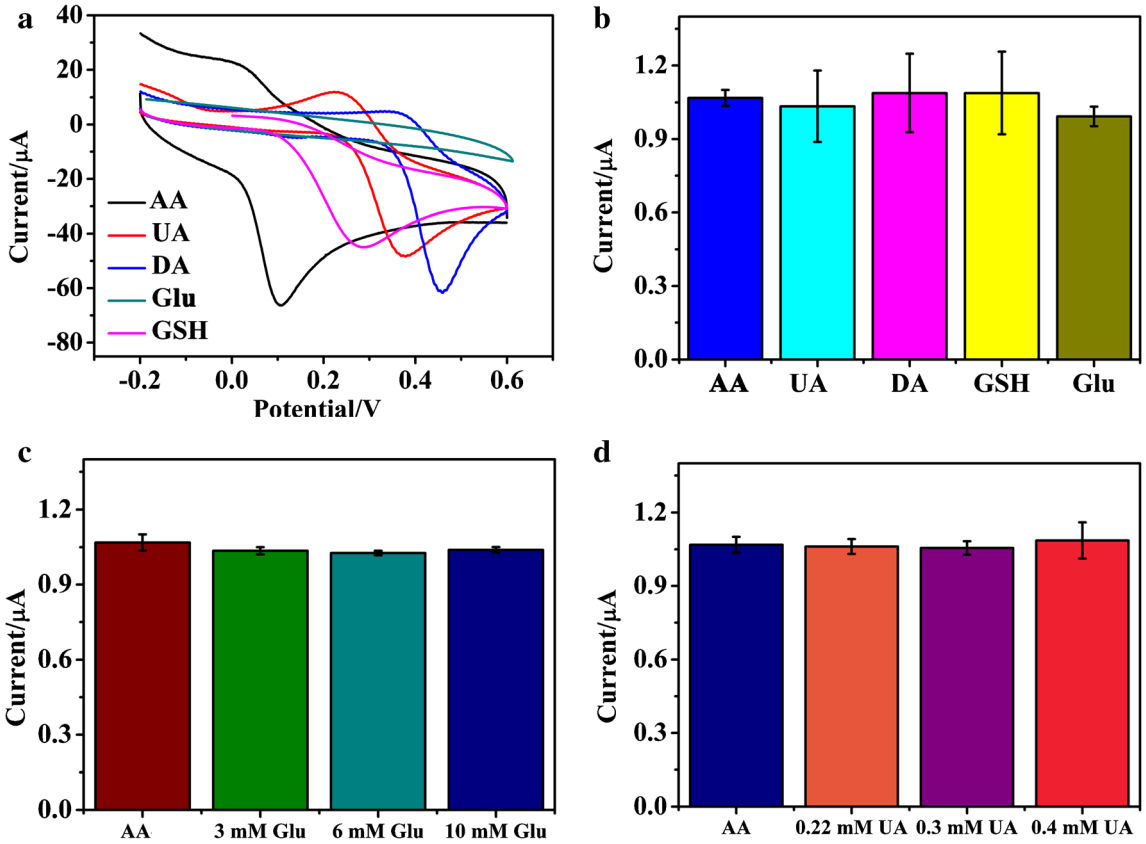

Fig. 7 **a** CVs recorded on the MWCNT/GO/AuNR/GCE in phosphate buffer (including 0.1 M NaCl, pH 7.4) at temperature 55 °C with 8 mM AA, UA, DA, Glu, or GSH. **b** Influence of addition of 1×10^{-6} M UA, DA, GSH or Glu on the oxidation peak current of AA with the same concentration at working potential of 0.036 V (vs. Ag/AgCl) by DPV. **c** Influence of addition of 3, 6 and 10 mM Glu on the oxidation peak current of 1×10^{-6} M AA at working potential of 0.036 V (vs. Ag/AgCl) by DPV. **d** Influence of addition of 0.22, 0.3 and 0.4 mM UA on the oxidation peak current of 1×10^{-6} M AA at working potential of 0.036 V (vs. Ag/AgCl) by DPV. Error bars show the standard deviation of three independent measurements

0.5091) ($R = 0.999$) (Fig. 4b). The result indicates that it is a typical adsorption-controlled reaction in the process of electrochemical oxidation of AA on MWCNT/GO/AuNR modified GCE surface. In addition, the linear relationship of the oxidation peak potential of AA (E_p) with the natural logarithm of scan rates (Inv) is revealed in Fig. S2 in Electronic Supporting Material. The electron transfer number and the heterogeneous electron transfer rate constant can be calculated to be 2.25 and 0.82 s^{-1}, respectively (Electronic Supporting Material). It indicates that the electrode process of AA at the hybrid modified electrode is not completely irreversible. The very small reduction peak appeared on CV of AA at MWCNT/GO/AuNR/GCE (Fig. 3b) confirms this point.

The determination of AA with MWCNT/GO/AuNR/GCE

In order to estimate the sensitivity of the presented sensor for the detection of AA, DPV was adopted to study peak current dependence on the concentration of AA. As can be seen from Fig. 5a, c, the oxidation peak currents increased when the concentration of AA increased. The oxidation peak current is linear with the concentration of AA in the lower (1 nM to 0.5 μM) and higher (1 μM to 8 mM) range at a low working potential of 0.036 V (vs. Ag/AgCl) (Fig. 5b, d). There are two good linear ranges with high correlation coefficient (the respective linear regression equations and correlation coefficient are shown in Fig. 5b, d). A very low detection limit 0.85 nM was calculated at a signal-to-noise ratio of 3 based on

Table 1 Results for determination of AA in human serum

Sample	Added (μM)	Found (μM)	Recovery (%)	RSD (%)(n = 3)
Diluted serum	100	91.59	91.59	1.98
	0.1	0.10625	106.25	3.50
	0.001	0.001014	101.40	1.03

the linear range at lower concentrations. It is superior to other reported sensors for AA detection (Table S1 in Electronic Supporting Material). And also the linear range of the modified electrode is wider or comparable to the range reported. The sensitivity for the determination of AA is found to be 7.61 $\mu A \cdot \mu M^{-1} \cdot cm^{-2}$ (based on the linear range from 1 nM to 0.5 μM). Considering the convenience of application, the demonstrated sensor for the detection of AA was conducted at room temperate (Fig. 6). Two wider liner ranges (from 0.1 μM to 10 μM (Fig. 6b) and from 10 μM to 8 mM (Fig. 6d)) at a working potential of 0.086 V (vs. Ag/AgCl) were also found. The calculated sensitivity is as high as 2.97 $\mu A \cdot \mu M^{-1} \cdot cm^{-2}$ and the detection limit is 87 nM (based on the linear range from 0.1 μM to 10 μM). It can be found that the overall electrocatalytic performance at room temperature is better or comparative than most of reported sensors for AA detection (Table S1 in Electronic Supporting Material).

Selectivity of sensor

AA analysis is generally interfered by UA, DA, Glu and GSH, so we choose these electroactive compounds to assess the selectivity performance of MWCNT/GO/AuNR/GCE. The electrochemical behaviors of different small molecules were demonstrated by CV at a concentration of 8 mM (Fig. 7a). Compared with AA, the detected interferential substances possess a large difference on oxidation potential, and Glu shows no obvious signal in phosphate buffer (including 0.1 M NaCl, pH 7.4). Figure 7b shows the influence of addition of 1×10^{-6} M UA, DA, GSH or Glu on the oxidation peak current of AA with the same concentration at working potential of 0.036 V (vs. Ag/AgCl) by DPV. It can be found that all added small molecules have no obvious effect on the current of AA. Moreover, even if the concentration of Glu is higher than 3 mM (Fig. 7c) or UA higher than 0.22 mM (Fig. 7d), the oxidation peak current of ascorbic acid was not affected obviously. The results indicate excellent selectivity of the prepared nanohybrid modified GCE for AA detection.

Real sample analysis

In order to investigate the practical application of the nanohybrid modified GCE, electrochemical determination of AA in biological sample such as human serum, was performed. The human serum was first diluted with phosphate buffer (including 0.1 M NaCl, pH 7.4), and known amount of standard AA (100 μM, 0.1 μM and 0.001 μM) was added into the diluted real samples, respectively and recovery rate was monitored. The results were demonstrated in Table 1. As can been seen, the recoveries ranged from 91.59%~101.40% with a relative standard deviation (RSD) of <3.50% ($n = 3$), exhibiting a promising application of MWCNT/GO/AuNR/GCE in the determination of AA in real samples.

Reproducibility and stability

In order to estimate the reproducibility of the sensor, three different electrodes were modified with MWCNT/GO/AuNR and used to detect AA with different concentration (Fig. 6b, d). We can found that the sensor exhibits excellent reproducibility for different modified GCE. Then stability was challenged using the modified electrode for different time. The current values were investigated at 5 μM AA every 2 days. After 9 days, the current response maintains about 93.68% of its initial current response and the RSD of the oxidation peak currents is 3.51%. Therefore, the sensor has a better stability and reproducibility for the detection of AA.

From above results and discussions, the sensor demonstrates excellent electrocatalytic performance at 55 °C. If it works at room temperature, the electrocatalytic performance declines. However, two wider linear range, lower detection limit and higher sensitivity are still promising for real application.

Conclusion

Herein, a sensing interface based on MWCNTs, GO and AuNRs is described that possesses a favorable electrocatalytic performance for AA. Unlike reported before, GO was used to disperse MWCNTs without subsequent reduction step. Positively charged AuNRs was dropped onto the MWCNT/GO modified GCE to produce synergistic action of MWCNT/GO and AuNRs. However, the method requires a working temperature of 55 °C. This is a disadvantage and restricts the applicability of the method in routine analysis although the electrocatalytical performance is still good at room temperature. On MWCNT/GO/AuNR modified GCE surface, AA oxidation underwent an adsorption-controlled reaction and shows poor reversibility. Despite these limitations, this work may have some reference value for assembling various nanomaterials onto the surface the MWCNT/GO film for wider applications such as in electrocatalysis and electroanalysis.

Acknowledgements This work was supported by the Natural Science Foundation of Shandong Province, China (Nos. ZR2016BM27 and ZR2017PB006).

Compliance with ethical standards The author(s) declare that they have no competing interests.

References

1. Hei Y, Li X, Zhou X, Liu J, Hassan M, Zhang S, Yang Y, Bo X, Wang HL, Zhou M (2018) Cost-effective synthesis of three-dimensional nitrogen-doped nanostructured carbons with hierarchical architectures from the biomass of sea-tangle for the amperometric determination of ascorbic acid. Anal Chim Acta 1029:15–23
2. Haldorai Y, Choe SR, Huh YS, Han YK (2018) A composite consisting of microporous carbon and cobalt(III) oxide and prepared from zeolitic imidazolate framework-67 for voltammetric determination of ascorbic acid. Microchim Acta 185:116
3. Scremin J, Barbosa ECM, Salamanca-Neto CAR, Camargo PHC, Sartori ER (2018) Amperometric determination of ascorbic acid with a glassy carbon electrode modified with TiO2-gold nanoparticles integrated into carbon nanotubes. Microchim Acta 185:251
4. Taleb M, Ivanov R, Bereznev S, Kazemi SH, Hussainova I (2017) Ultra-sensitive voltammetric simultaneous determination of dopamine, uric acid and ascorbic acid based on a graphene-coated alumina electrode. Microchim Acta 184:4603–4610
5. Wu F, Huang T, Hu Y, Yang X, Ouyang Y, Xie Q (2016) Differential pulse voltammetric simultaneous determination of ascorbic acid, dopamine and uric acid on a glassy carbon electrode modified with electroreduced graphene oxide and imidazolium groups. Microchim Acta 183:2539–2546
6. Mallikarjuna K, Reddy YVM, Sravani B, Madhavi G, Kim H, Agarwal S, Gupta VK (2018) Simple synthesis of biogenic Pd-ag bimetallic nanostructures for an ultrasensitive electrochemical sensor for sensitive determination of uric acid. J Electroanal Chem 822: 163–170
7. Yadav DK, Gupta R, Ganesan V, Sonkar PK (2017) Individual and simultaneous voltammetric determination of ascorbic acid, uric acid and folic acid by using a glassy carbon electrode modified with gold nanoparticles linked to bentonite via cysteine groups. Microchim Acta 184:1951–1957
8. Cumings J, Zettl A (2000) Low-friction nanoscale linear bearing realized from multiwall carbon nanotubes. Science 289:602–604
9. Treacy MMJ, Ebbesen TW, Gibson JM (1996) Exceptionally high Young's modulus observed for individual carbon nanotubes. Nature 381:678–680
10. Noked M, Okashy S, Zimrin T, Aurbach D (2012) Composite carbon nanotube/carbon electrodes for electrical double-layer super capacitors. Angew Chem Int Ed 51:1568–1571
11. You B, Jiang JH, Fan SJ (2014) Three-dimensional hierarchically porous all-carbon foams for supercapacitor. ACS Appl Mater Interfaces 6:15302–15308
12. Cote LJ, Kim J, Tung VC, Luo JY, Kim F, Huang JX (2011) Graphene oxide as surfactant sheets. Pure Appl Chem 83:95–110
13. Kim J, Cote LJ, Kim F, Yuan W, Shull KR, Huang JX (2010) Graphene oxide sheets at interfaces. J Am Chem Soc 132:8180–8186
14. Cao F, Huang YK, Wang F, Kwak D, Dong QC, Song DH, Zeng J, Lei Y (2018) A high-performance electrochemical sensor for biologically meaningful L-cysteine based on a new nanostructured L-cysteine electrocatalyst. Anal Chim Acta 1019:103–110
15. Rocha DP, Silva MNT, Cardoso RM, Castro SVF, Tormin TF, Richter EM, Nossol E, Munoz RAA (2018) Carbon nanotube/reduced graphene oxide thin-film nanocomposite formed at liquid-liquid interface: characterization and potential electroanalytical applications. Sensor Actuat B-Chem 269:293–303
16. Zhu YW, Murali S, Cai WW, Li XS, Suk JW, Potts JR, Ruoff RS (2010) Graphene and graphene oxide: synthesis, properties, and applications. Adv Mater 22:3906–3924
17. Xu H, Li Q, Wang LH, He Y, Shi JY, Tang B, Fan CH (2014) Nanoscale optical probes for cellular imaging. Chem Soc Rev 43: 2650–2661
18. Uhm S, Tuyen NH, Lee J (2011) Controlling oxygen functional species of graphene oxide for an electro-oxidation of L-ascorbic acid. Electrochem Commun 13:677–680
19. Xiong H, Jin BK (2011) The electrochemical behavior of AA and DA on graphene oxide modified electrodes containing various content of oxygen functional groups. J Electroanal Chem 661:77–83
20. Zhang DJ, Xu CY, Li SJ, Zhang RC, Yan HL, Miao HJ, Fan Y, Yuan BQ (2014) Electrochemically controlling oxygen functional groups in graphene oxide for the optimization in the electrocatalytic oxidation of dihydroxybenzene isomers and L-methionine. J Electroanal Chem 717:219–224
21. Alagiri M, Rameshkumar P, Pandikumar A (2017) Gold nanorod-based electrochemical sensing of small biomolecules: a review. Microchim Acta 184:3069–3092
22. Yuan B, Xu C, Deng D, Xing Y, Liu Y, Pang H, Zhang D (2013) Graphene oxide/nickel oxide modified glassy carbon electrode for supercapacitor and nonenzymatic glucose sensor. Electrochim Acta 88:708–712
23. Yuan B, Xu C, Liu L, Zhang Q, Ji S, Pi L, Zhang D, Huo Q (2013) Cu_2O/NiO_x/graphene oxide modified glassy carbon electrode for the enhanced electrochemical oxidation of reduced glutathione and nonenzyme glucose sensor. Electrochim Acta 104:78–83
24. Hummers WS, Offeman RE (1958) Preparation of graphitic oxide. J Am Chem Soc 80:1339
25. Sau TK, Murphy CJ (2004) Seeded high yield synthesis of short au nanorods in aqueous solution. Langmuir 20:6414–6420
26. Wang QB, Liu SB, Fu LY, Cao ZS, Ye WN, Li HL, Guo PZ, Zhao XS (2018) Electrospun gamma-Fe_2O_3 nanofibers as bioelectrochemical sensors for simultaneous determination of small biomolecules. Anal Chim Acta 1026:125–132
27. Bagheri H, Pajooheshpour N, Jamali B, Amidi S, Hajian A, Khoshsafar H (2017) A novel electrochemical platform for sensitive and simultaneous determination of dopamine, uric acid and ascorbic acid based on Fe3O4-SnO2-gr ternary nanocomposite. Microchem J 131:120–129
28. Sun CL, Chang CT, Lee HH, Zhou JG, Wang J, Sham TK, Pong WF (2011) Microwave-assisted synthesis of a core-Shell MWCNT/GONR heterostructure for the electrochemical detection of ascorbic acid, dopamine, and uric acid. ACS Nano 5:7788–7795
29. Sajid M, Nazal MK, Mansha M, Alsharaa A, Jillani SMS, Basheer C (2016) Chemically modified electrodes for electrochemical detection of dopamine in the presence of uric acid and ascorbic acid: a review. Trac-Trend Anal Chem 76:15–29
30. Dong Q, Song D, Huang Y, Xu Z, Chapman JH, Willis WS, Li B, Lei Y (2018) High-temperature annealing enabled iridium oxide nanofibers for both non-enzymatic glucose and solid-state pH sensing. Electrochim Acta 281:117–126
31. Nikoobakht B, El-Sayed MA (2003) Preparation and growth mechanism of gold nanorods (NRs) using seed-mediated growth method. Chem Mater 15:1957–1962
32. Hu XB, Yu Y, Hou WM, Zhou JE, Song LX (2013) Effects of particle size and pH value on the hydrophilicity of graphene oxide. Appl Surf Sci 273:118–121
33. Borthakur P, Boruah PK, Hussain N, Sharma B, Das MR, Matic S, Reha D, Minofar B (2016) Experimental and molecular dynamics simulation study of specific ion effect on the graphene oxide surface and investigation of the influence on reactive extraction of model dye molecule at water-organic interface. J Phys Chem C 120: 14088–14100
34. Mathur A, Roy SS, McLaughlin JA (2010) Transferring vertically aligned carbon nanotubes onto a polymeric substrate using a hot

embossing technique for microfluidic applications. J R Soc Interface 7:1129–1133

35. Mani V, Devadas B, Chen SM (2013) Direct electrochemistry of glucose oxidase at electrochemically reduced graphene oxide-multiwalled carbon nanotubes hybrid material modified electrode for glucose biosensor. Biosens Bioelectron 41:309–315